Study on Extracting Precipitation Information Using Infrared Bands of Himawari-8

Yuko Kishida (1), Keiji Imaoka (1), Hidenori Shingin (1), Kakuji Ogawara (1)

[1] Yamaguchi University, 16-1 Tokiwadai 2-chome, Ube-shi, Yamaguchi, 755-8611, Japan
Email: i017vd@yamaguchi-u.ac.jp; k.imaoka@yamaguchi-u.ac.jp;
shingin@yamaguchi-u.ac.jp; ogawara@yamaguchi-u.ac.jp

KEY WORDS: Himawari-8, brightness temperatures, rainfall

ABSTRACT: Heavy rains occur every year in Japan and often cause disasters. Therefore, there is a great concern for heavy rain in the field of disaster prevention. Although it is not possible to directly observe rainfall in visible and infrared wavelength, geostationary meteorological satellites have an advantage of observing the wide area with high frequency. Since Himawari-8 began its observation, it became possible to observe the area of Japan with high frequency of every 2.5 minutes. In this study, we analyzed the characteristics of precipitating clouds formed in Japan area using brightness temperatures (Tbs) obtained through an infrared band of Himawari-8 at 2 sides of time information and multi band information. First, we performed temporal analysis of cloud-top Tbs using one-year data from band 13 (10.4 μm) observation. We identified and tracked isolated precipitating clouds with the Tb threshold of 235 K and examined the time variations of cloud-top Tbs and areas. At the same time, we used rainfall from XRAIN, and investigated the time variation. In the early phase after the detection of precipitating clouds, we observed decreasing trend of cloud-top Tbs. The gradient of the decrease showed a relationship with the duration and the total amount of rainfall. The longer the duration and the larger the total amount of rainfall, the steeper gradient we observed. This indicates that the size of the gradient, which corresponds to the difference of vertical growth rate, affects the rainfall in the later stage. Therefore, time variation information with short time interval can provide useful information to estimate precipitation from Himawari-8 data. Next, we analyzed multiband information by Himawari-8. To avoid the effect of orographic rainfall and simply our analysis, we selected relatively flat region over the Kanto area. We extracted 61×61 pixels subset (35.3°N~36.5°N, 139.4°E~140.6°E) from Himawari-8 data at 10 infrared bands under the condition that over 50 % of the subset area was with rainfall. Before computing the statistics, the XRAIN rainfall rate were spatially averaged over the Himawari-8 grid size (2 km). The information related to cloud-top height and optical depth in atmospheric window and water vapor bands indicated some relationships with rainfall rate, but not much for judging rain/no-rain situations. We would like to investigate for further details and expand this result to the development of deep-learning estimation of heavy rainfall events. At the conference, updated results will be presented and discussed.

1. INTRODUCTION

Heavy rains occur every year in Japan and often cause disasters. Therefore, there is a great concern for heavy rain in the field of disaster prevention. To reduce human damages, the Japan Meteorological Agency (JMA) reformed how to announce the weather information of disaster prevention this year (JMA, 2019). For delivering the reliable weather information, continuous and frequent observation of precipitation is necessary. In Japan, radar rain gauges are installed all over the country and provide frequent observations. For example, the eXtended RAdar Information Network (XRAIN), which owned by Ministry of Land, Infrastructure, Transport and Tourism (MLIT), is delivering the precipitation information in near-real time. However, there are many

areas in the world where radar rain gauges and meteorological observation stations are not densely installed. Also, observations with radar rain gauges are limited to land areas. Satellite remote sensing techniques have been used for global and unbiased precipitation measurement. Microwave instruments can provide direct information of precipitation layer. However, they are only onboard polar orbiting satellites and the observation frequency is about twice a day. On the other hand, visible and infrared instruments can be installed on geostationary satellites and are good at frequent observation. Although visible and infrared instruments are not able to obtain precipitation information directly, indirect estimation is still possible through the cloud information such as optical thickness and cloud top height.

Since Himawari-8 began its observation on July 7, 2015, it became possible to observe the entire Earth as seen from the satellite (hereafter called Full-Disk) every 10 minutes, and the area of Japan with every 2.5 minutes. The number of bands increased from 5 to 16 and the horizontal resolution was improved from 4 to 2 km in infrared bands compared to the predecessor imager on the MTSAT series. Since precipitating clouds that cause heavy rain like cumulonimbus develop in a short time, observations with short time interval like by Himawari-8 can provide useful information for estimating precipitation. Also, the increased spectral information may help improve the accuracy. In this study, we investigated the temporal and spectral characteristics of precipitating clouds over the Kanto area in Japan by using Himawari-8 brightness temperatures (Tbs) and rain information from XRAIN.

2. INSTRUMENTS AND DATA

2.1 Himawari-8

The Advanced Himawari Imager (AHI) on Himawari-8 is composed of 3 visible bands, 3 near infrared bands, and 10 infrared bands. We used only infrared bands of Himawari-8/AHI. Table 1 shows the specification of infrared bands of Himawari-8 (Meteorological Satellite Center (MSC) of JMA, 2013).

For the temporal analysis, we used Tbs at Band 13 over Japan area with 2.5-minutes interval from August 1, 2016 to July 31, 2017 (UTC). We obtained NetCDF files from the National Institute of Information and Communications Technology (NICT) Science Cloud. For the spectral analysis, we downloaded Full-Disk NetCDF files with 10-minutes interval from January 1, 2018 to December 31, 2019 (UTC) from the Japan Aerospace Exploration Agency (JAXA) Himawari Monitor.

Table 1. Specification of infrared bands of Himawari-8

Band number	Spatial resolution [km]	Central wave length [μm]
7	2	3.8853
8	2	6.2429
9	2	6.9410
10	2	7.3467
11	2	8.5926
12	2	9.6372
13	2	10.4073
14	2	11.2395
15	2	12.3806
16	2	13.2807

2.2 XRAIN

When XRAIN started data distribution in 2010, it was based on X-band MP radar rain gauges. Since 2016, it tentatively started distribution using combined data of X-band and C-band MP radar rain gauges. As summarized in Table 2, the X-band and C-band MP radar rain gauges that are used in XRAIN have different features (Terakawa 2017). As of 2017, MLIT had installed 39 and 14 of X-band and C-band MP radar rain gauges, respectively, as seen in Table 2. Synthesizing the X- and C-band data can make up for each other's weak points.

We downloaded XRAIN data from the XRAIN Realtime Precipitation Data of the Data Integration and Analysis System (DIAS). On this system, XRAIN data is created using X-band MP radar data until the end of May 2018 (JST) and using X- and C-band MP radar data from June 2018 (JST). For the temporal analysis, data over the Kanto area (34.6666 ° N~38.0000 ° N, 138.0000°E~142.0000°E) with 5-minutes interval were used. For the spectral analysis, we used subset data from the Kanto area with 10-minutes interval from May 1 to December 31, 2018 (JST). In addition, we supplemented the data conforming with the period of Himawari-8 data.

Table 2. Features of X-band and C-band MP radar rain gauges

Type of radar rain gauge	C-band	X-band
Polarization	horizontal polarization and vertical polarization	
Frequency	5.2 ~ 5.4 GHz	9.7 ~ 9.8 GHz
Spatial resolution	250m	
Observation interval	1 minute	
Limit of quantitative observation	120 km radius	60 km radius
Revision using ground rain gauge	Unnecessary	
Installation location (number)	Mountains (14)	Flatland (39)
Observation range	All of Japan (developing)	Important areas

3. TEMPORAL ANALYSIS

3.1 Methods

We analyzed the temporal evolution of precipitating clouds to examine the advantages of high frequency observation like by Himawari-8 in estimating precipitation information. We investigated the relationship between evolution stages identified by the cloud tracking method with 2.5 minutes interval and several parameters of precipitating clouds including areas, cloud-top Tbs, and rainfall rates by XRAIN over the area of Japan (rainfall rates were only available over the Kanto area). The cloud tracking method we used was similar to that in the previous paper (Kondo et al., 2006). Band 13, located within the atmospheric window region, was used to measure cloud-top Tbs as the indicator of cloud-top height. When Tb value in a pixel was 235 K or less, we considered the pixel as a cold cloud. Then, we performed four-neighbor labeling on this pixel and defined the connected cold-cloud area. We considered this cold-cloud area as a precipitating cloud. The threshold value of 235 K was used in some studies that estimated precipitation using infrared data of geostationary meteorological satellite (Arkin, 1979 and Xie et al., 1991). We calculated several parameters for this precipitating cloud including the geometric center latitude and longitude, cloud area, averaged Tb, and minimum Tb. We did not apply the threshold value to the cloud area and judged as a precipitating cloud even one pixel. If the precipitating cloud was included in Kanto area of XRAIN, we calculated XRAIN averaged rainfall rate in the precipitating cloud. Next, we defined a set of temporally continuous precipitating

clouds in consecutive data as a precipitating cloud system. We examined the distance between precipitating clouds in two consecutive data and we decided as continuous precipitating clouds when the distance was 10 km or less after 2.5 minutes. We repeated this procedure for the next two consecutive data in sequence until the continuation was terminated. When single (multiple) precipitating cloud (clouds) encountered multiple (single) precipitating clouds (cloud) within the threshold distance after 2.5 minutes, we defined that the splitting (merging) process occurred. Although some precipitating clouds show complex development process like repeated splitting and merging in reality, we excluded those processes to simplify our analysis. The threshold distance of 10 km was decided by taking the cloud movement due to wind into consideration. The moving velocity of 60 m s^{-1} in the similar study (Machado et al., 1998) was converted to the moving distance in 2.5 minutes and approximated. In this study, we did not evaluate the validity of thresholds for cloud area and distance. Finally, we sorted precipitating cloud systems by duration time and calculated the precipitating cloud parameters and XRAIN averaged rainfall rate for each precipitation cloud system.

3.2 Results and discussion

3.2.1 Precipitation cloud parameters: Figure 1 shows the time evolution of precipitating cloud parameters and XRAIN averaged rainfall rate averaged over one year. Different colors indicate the duration times from 30 to 180 minutes with 30 minutes interval. The horizontal axes are time [min] for all panels and the vertical axes are averaged Tb [K], minimum Tb [K], cloud area [km^2], and XRAIN averaged rainfall rate [mm h^{-1}]. In general, the time evolution curves for different duration times exhibit similar figure for the precipitating cloud parameters. Regardless of the duration time, precipitating clouds may develop vertically at early stage and exhibit Tb decrease. At the tropopause, they may expand parallel to the horizon and gradually dissipate, resulting in the Tb increase and area expansion at the same time. Although the XRAIN averaged rainfall rate significantly fluctuate because of the small number of samples, we can still confirm some tendencies. For example, the rainfall rate tends to represent the maximum value at early stage and decrease with time. Also, the precipitating cloud system with longer duration time tends to have larger initial maximum value.

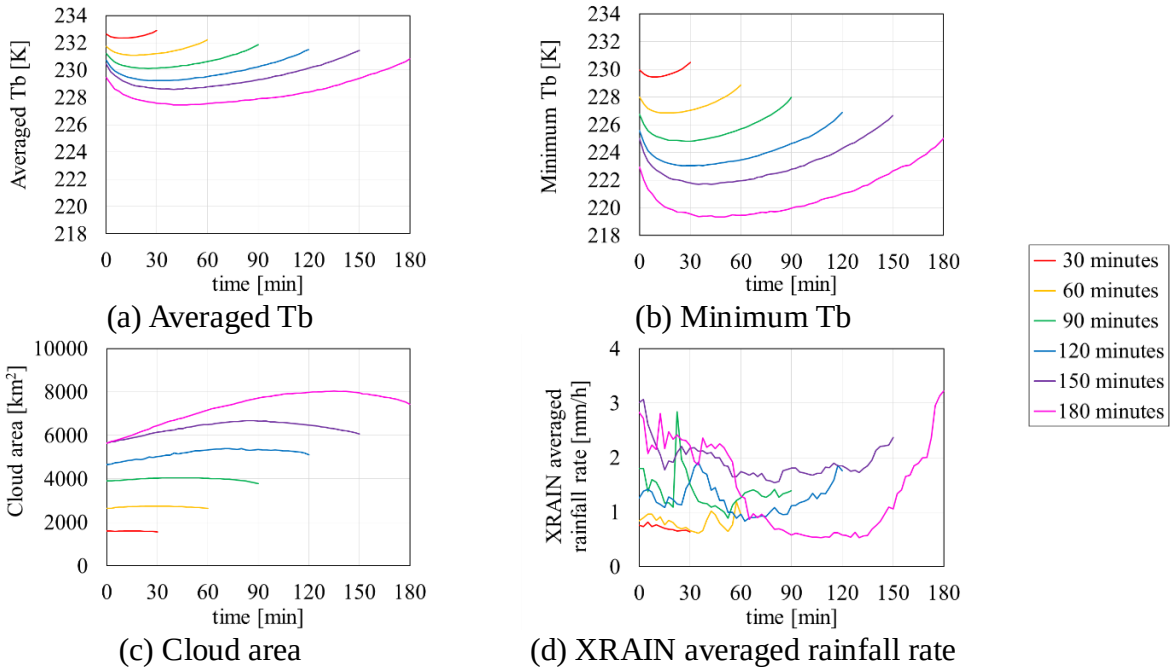

Figure 1. Temporal change of precipitation cloud parameters

3.2.2 XRAIN total precipitation amount: Figure 2 shows the XRAIN total rainfall amount during the duration time as a function of initial Tb value and cloud area in Fig. 1. In Fig. 2 (a), the horizontal axis is the initial Tb value [K] and the vertical axis is the XRAIN total precipitation amount [mm]. In Fig. 2 (b), the horizontal axis is the initial value of cloud area [km^2] and the vertical axis is XRAIN total precipitation amount during the duration time [mm]. When we focus on the initial Tb value in Fig. 1 (a), the longer the duration time, the smaller the initial Tb value. In Fig. 2 (a), we can see that the XRAIN total rainfall amount increases with decrease of the initial Tb value. This leads to the fact that the precipitating cloud system with lower initial Tb value tends to develop into longer and larger system with larger total rainfall amount. In addition, from Fig. 1 (a) and (b), we can confirm that the smaller the initial Tb value, the larger the Tb decreasing rate at early stage, indicating rapid vertical development. Based on the evidences above, we can speculate that the vertical development rate of precipitating clouds at the early stage and the total rainfall amount during the duration time are closely related. Therefore, observing Tbs with short-time interval like by Himawari-8 could provide useful information to estimate precipitation information.

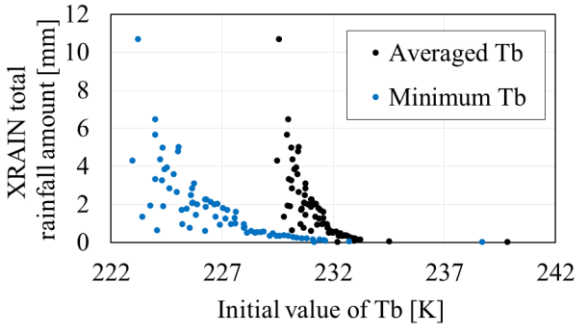

(a) Initial Tb value and total rainfall amount

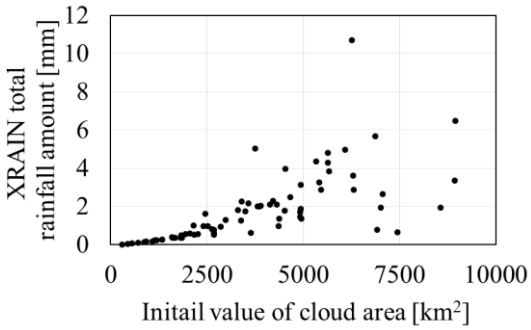

(b) Initial value of cloud area and total rainfall amount

Figure 2. Comparisons between initial values of precipitating cloud parameters and XRAIN total rainfall amount

4. SPECTRAL ANALYSIS

4.1 Methods

In this analysis, we investigate the relationship between multiband Tbs and rainfall rate to examine if the multiband information by Himawari-8 is useful for estimating precipitation information. To avoid the effect of orographic rainfall and simply our analysis, we selected relatively flat region over the Kanto area. We extracted 61×61 pixels subset (35.3°N~36.5°N, 139.4°E~140.6°E) from Himawari-8 data at 10 infrared bands under the condition that over 50 % of the subset area was with rainfall. Before computing the statistics, the XRAIN rainfall rate were spatially averaged over the Himawari-8 grid size (2 km). We summarized the statistics in the form of two-dimensional diagrams.

4.2 Results and discussion

4.2.1 Using the atmospheric window and water vapor bands : Figure 3 shows averaged rainfall rate and occurrence frequency of rain/no-rain as a function of Tbs at Band 13 and 10. Band 13 and 10 were selected to represent the atmospheric window and water vapor bands,

respectively. In Fig. 3 (a), heavy rainfall tends to occur when Tbs of both bands are within the range between 200 and 220 K. This is consistent with the previous study (Xie et al., 1991). In Fig. 3 (b) and (c), the distribution of occurrence frequency does not show large difference between rain and no-rain cases.

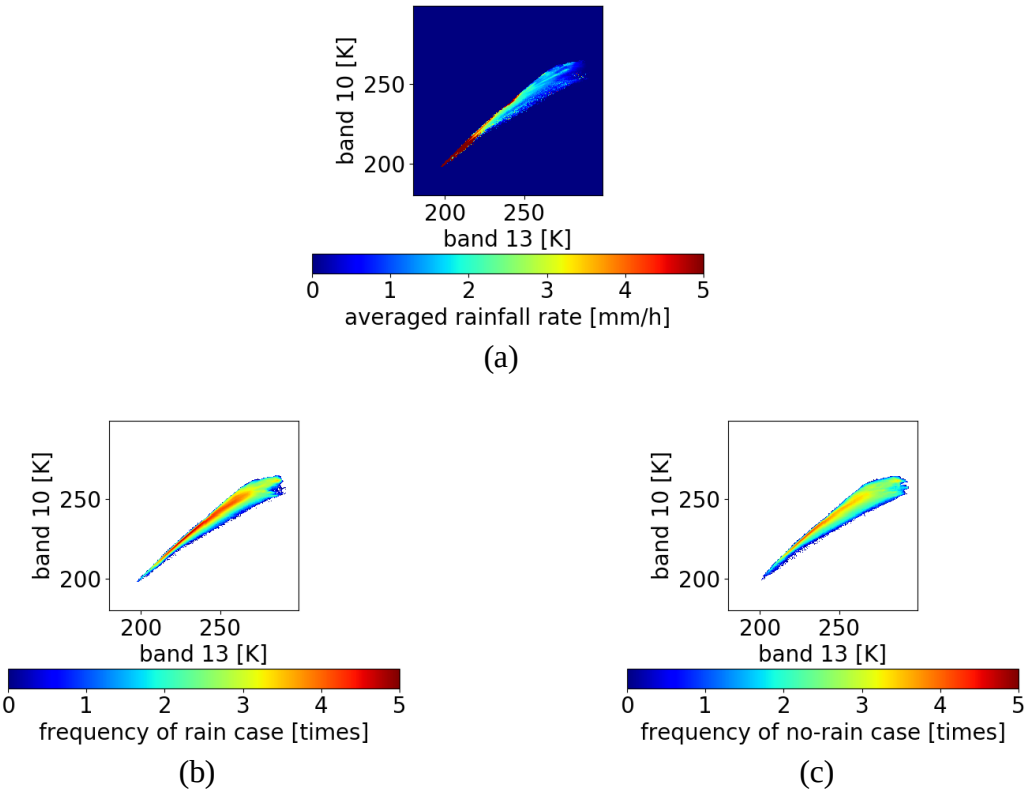

Figure 3. Two dimensional diagrams of (a) averaged rainfall rate [mm h^{-1}], (b) occurrence frequency of rain case with common logarithm, and (c) occurrence frequency of no-rain case with common logarithm, as a function of Tbs at Band 13 and 10 using 2018 data (horizon axis: Band 13, vertical axis: Band 10).

4.2.2 Using water vapor bands: Figures 4 and 5 show averaged rainfall rate and occurrence frequency of rain/no-rain cases as a function of Tb difference between two bands. As shown in Hirose et al. (2019), the Tb difference between Band 13 and 15 is used for split-window technique, and the differences between Band 9 and 10 and Band 8 and 9 are known as effective indices to judge water vapor amount. Panels (a), (c), and (e) in Fig. 4 and 5 are the cases with lower cloud-top height (Band 13 Tb > 252 K), and panels (b), (d), and (f) with higher cloud-top height (Band 13 Tb $\leqq$ 252 K). As seen in the panels (a) and (b) of both figures, averaged rainfall rate shows different distribution with cloud top height. The panels (a) in Fig. 4 and 5 show different result compared to the existing study (Hirose et al., 2019), which used larger study areas over land near Japan (20°N~50°N, 120°E~150°E) and different year and seasons. Such differences could lead to the different result. In panels (b) of Fig. 4 and 5, we can see that heavy rainfalls tend to gather around the coordinate origin. This tendency might be useful for detecting heavy rain. Regarding the slight concentration of heavy rainfall rate around the coordinates (10, -5) in panels (b), where the corresponding occurrence frequency in panels (d) are relatively low, we need to further investigate the reason. The occurrence frequency distribution does not show large difference between rain and no-rain cases in the panels (c), (e) and (d), (f), except the absolute number of times. This implies that these spectral differences may not provide significant information for

classifying rain and no-rain cases.

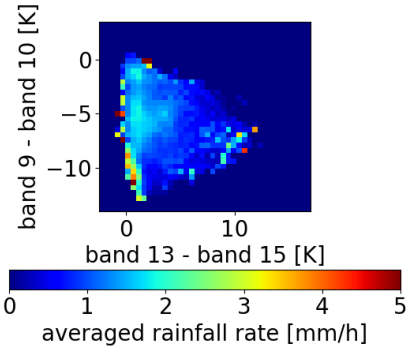

(a) Distribution map of averaged rainfall rate (band 13 > 252 K)

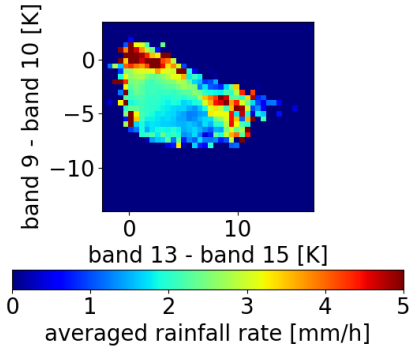

(b) Distribution map of averaged rainfall rate (band 13 ≦ 252 K)

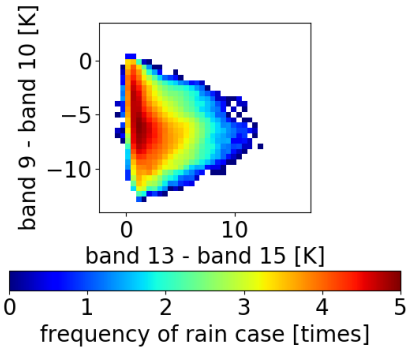

(c) Frequency distribution map of rain case (band 13 > 252 K)

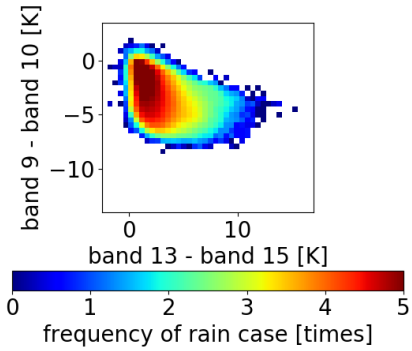

(d) Frequency distribution map of rain case (band 13 ≦ 252 K)

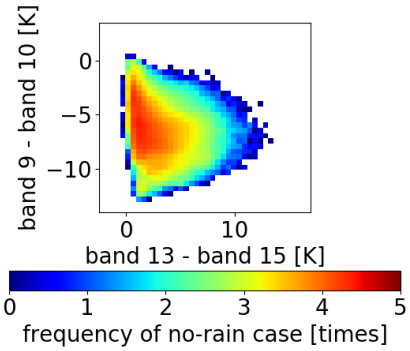

(e) Frequency distribution map of no-rain case (band 13 > 252 K)

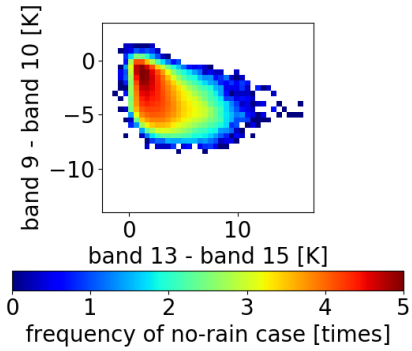

(f) Frequency distribution map of no-rain case (band 13 ≦ 252 K)

Figure 4. Top, middle, and bottom panels show two dimensional diagrams of averaged rainfall rate [mm h^{-1}], occurrence frequency of rain case, and occurrence frequency of no-rain case, respectively, as a function of Tb difference between two bands using 2018 data (horizon axis: Band 13 - Band 15, vertical axis: Band 9 - Band 10). Occurrence frequencies are expressed with common logarithm. Panels in left and right columns show the diagrams for lower and higher cloud-top height, respectively, by using Band 13 Tbs with threshold of 252 K.

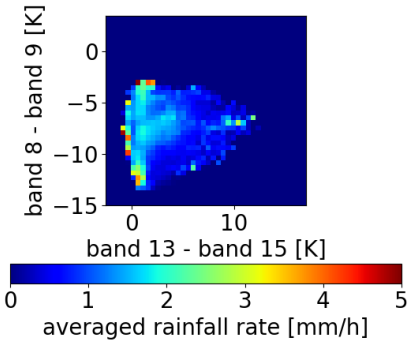

(a) Distribution map of averaged rainfall rate (band 13 > 252 K)

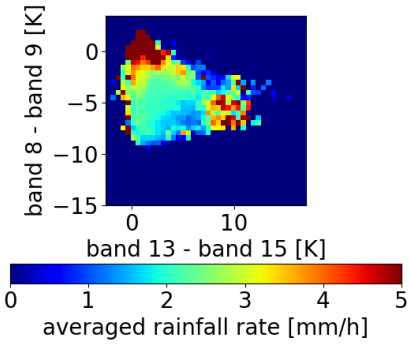

(b) Distribution map of averaged rainfall rate (band 13 ≦ 252 K)

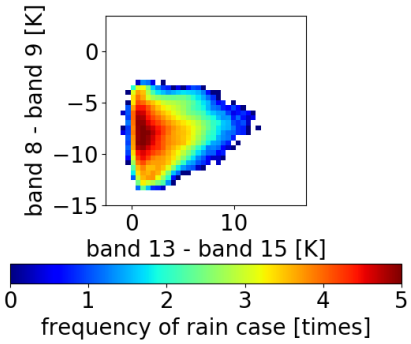

(c) Frequency distribution map of rain case (band 13 > 252 K)

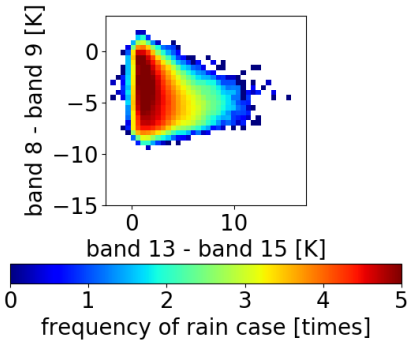

(d) Frequency distribution map of rain case (band 13 ≦ 252 K)

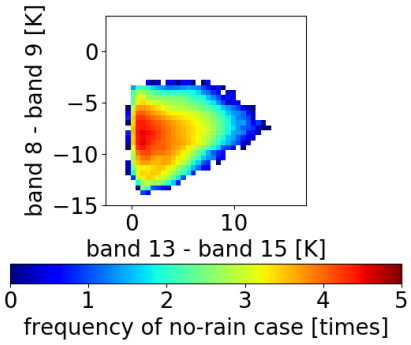

(e) Frequency distribution map of no-rain case (band 13 > 252 K)

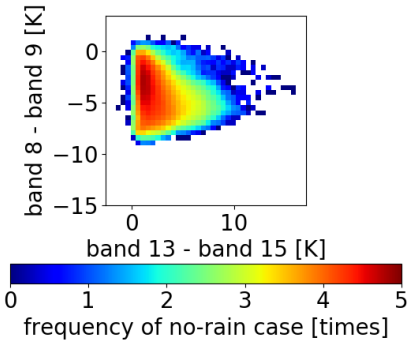

(f) Frequency distribution map of no-rain case (band 13 ≦ 252 K)

Figure 5. Same as Fig. 4, but Tb difference between Band 8 and 9 is used for vertical axis.

5. CONCLUSION

We analyzed temporal and spectral information of Himawari-8/AHI infrared Tbs and XRAIN rainfall rate for precipitating clouds over Japan to examine the potential advantages of Himawari-8 observations for estimating precipitation information. In the temporal analysis, we found for precipitating cloud systems identified by AHI Band 13 Tbs the relationship between vertical growth rate at early stage and total amount of rainfall within the duration time. This may provide the additional information for early detection of heavy rain. The short-time interval measurement by Himawari-8 is important for this purpose. The spectral analysis showed some potential

advantages of multiband information provided by Himawari-8. The information related to cloud-top height and optical depth in atmospheric window and water vapor bands indicated some relationships with rainfall rate, but not much for judging rain/no-rain situations. We would like to investigate for further details and expand this result to the development of deep-learning estimation of heavy rainfall events.

REFERENCES

Hirose, H., Shige, S., Yamamoto, M. K., and Higuchi, A., 2019. High temporal rainfall estimations from Himawari-8 multiband observations using the random-forest machine-learning method. Journal of the Meteorological Society of Japan, 97 (3), pp. 689-710.

Japan Meteorological Agency (JMA), 2019. About immediate approach for improvement how to announce weather information of disaster prevention, Retrieved September 1, 2019, from https://www.jma.go.jp/jma/press/1905/29a/20190529_tsutaekata_torikumi.html

Meteorological Satellite Center (MSC) of JMA, 2013. Imager (AHI), Retrieved September 1, 2019, from http://www.data.jma.go.jp/mscweb/en/himawari89/space_segment/spsg_ahi.html

Terakawa, A., 2017. About securing and improving quality for synthesis data of radar rain gauges, Retrieved February 20, 2018, from http://www.river.or.jp/01kenshuu/tech/tech23/result.html

Kondo, Y., Higuchi, A., and Nakamura, K., 2006. Small-scale cloud activity over the maritime continent and the western pacific as revealed by satellite data. Monthly Weather Review, 134 (6), pp. 1581-1599.

Arkin, P. A., 1979. The relationship between fractional coverage of high cloud and rainfall accumulations during GATE over the B-scale array. Monthly Weather Review, 107 (10), pp. 1382-1387.

Xie, P., and Mitsuta, Y., 1991. Rainfall estimation from GMS infrared imagery data. Disaster Prevention Research Institute Annuals. B, 34 (B-1), pp.1-11.

Machado, L. A. T., Rossow, W. B., Guedes, R. L., and Walker A. W., 1998 Life cycle variations of mesoscale convective systems over the Americas. Monthly Weather Review, 126 (6), pp. 1630-1654.

ACKNOWLEDGEMENT

Himawari-8 data from“Himawari Data Archive” and “Himawari-8 Real Time Data and Past Data” were provided by the NICT Science Cloud. The Himawari-8 L1 gridded data for Full-Disk area were supplied by the P-Tree System, JAXA. XRAIN data from “XRAIN Realtime Precipitation Data” were produced by DIAS (Data Integration and Analysis System).